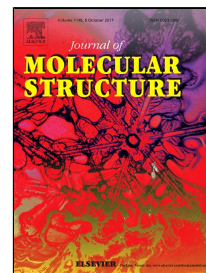


Accepted Manuscript

Synthesis, crystal structures, quantum chemical studies and corrosion inhibition potentials of 4-(((4-ethylphenyl)imino)methyl)phenol and (E)-4-((naphthalen-2-ylimino) methyl) phenol Schiff bases



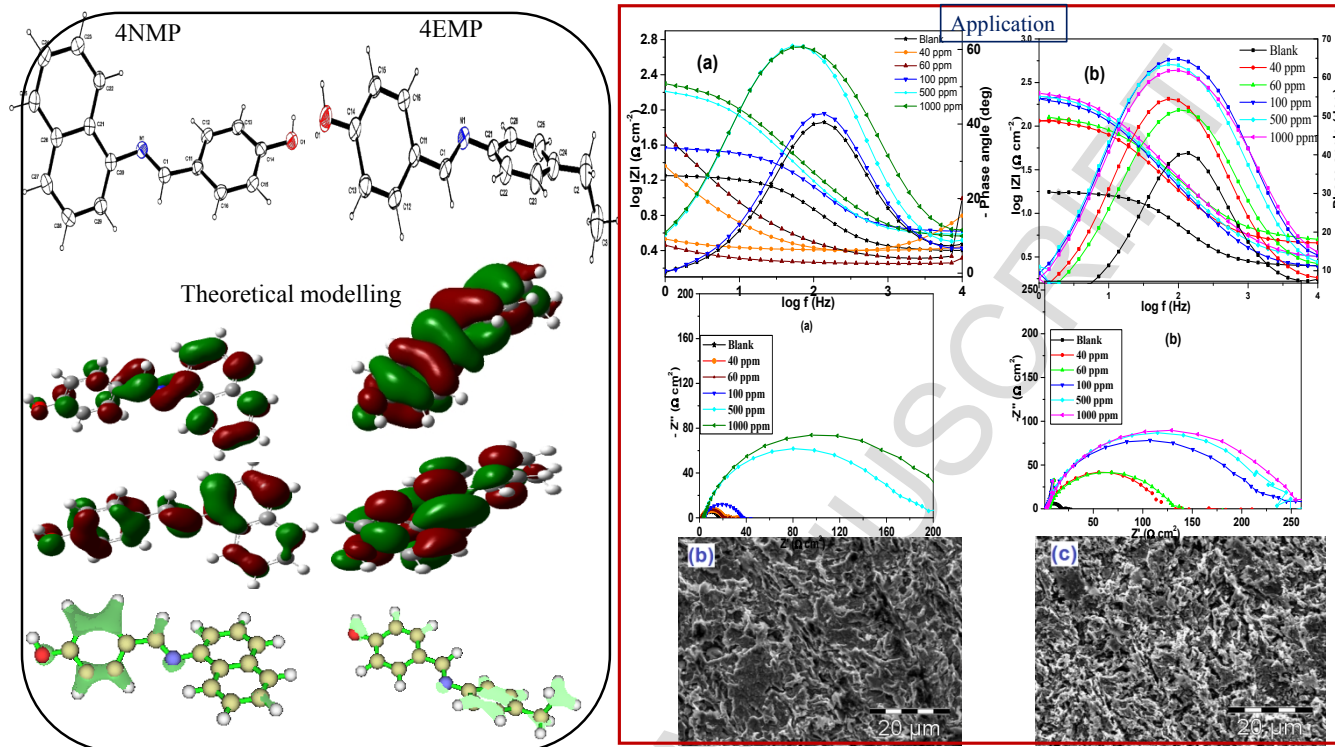
Elias E. Elemike, Henry U. Nwankwo, Damian C. Onwudiwe, Eric C. Hosten

PII: S0022-2860(17)30885-2
DOI: 10.1016/j.molstruc.2017.06.104
Reference: MOLSTR 23990
To appear in: *Journal of Molecular Structure*
Received Date: 13 May 2017
Revised Date: 20 June 2017
Accepted Date: 21 June 2017

Please cite this article as: Elias E. Elemike, Henry U. Nwankwo, Damian C. Onwudiwe, Eric C. Hosten, Synthesis, crystal structures, quantum chemical studies and corrosion inhibition potentials of 4-(((4-ethylphenyl)imino)methyl)phenol and (E)-4-((naphthalen-2-ylimino) methyl) phenol Schiff bases, *Journal of Molecular Structure* (2017), doi: 10.1016/j.molstruc.2017.06.104

This is a PDF file of an unedited manuscript that has been accepted for publication. As a service to our customers we are providing this early version of the manuscript. The manuscript will undergo copyediting, typesetting, and review of the resulting proof before it is published in its final form. Please note that during the production process errors may be discovered which could affect the content, and all legal disclaimers that apply to the journal pertain.

GRAPHICAL ABSTRACT



Synthesis, crystal structures, quantum chemical studies and corrosion inhibition potentials of 4-(((4-ethylphenyl)imino)methyl)phenol and (E)-4-((naphthalen-2-ylimino)methyl) phenol Schiff bases

^{1,2,3} Elias E. Elemike, ^{1,2}Henry U. Nwankwo, ^{1,2}Damian C. Onwudiwe*, ⁴Eric C. Hosten

1. Material Science Innovation and Modelling (MaSIM) Research Focus Area, Faculty of Agriculture, Science and Technology, North-West University, Mafikeng Campus, Private Bag X2046, Mmabatho 2735, South Africa.
2. Department of Chemistry, School of Mathematics and Physical Sciences, Faculty of Agriculture, Science and Technology, North-West University, Mafikeng Campus, Private Bag X2046, Mmabatho 2735, South Africa.
3. Department of Chemistry, College of Science, Federal University of Petroleum Resources, P.M.B 1221, Effurun, Delta State, Nigeria.
4. Department of Chemistry, Nelson Mandela Metropolitan University, P.O. Box 77000, Port Elizabeth 6031, South Africa

* Corresponding author

Email: Damian.Onwudiwe@nwu.ac.za

Tel: +27 18 - 389 -2545

Fax: +2718 – 389 -2420

Abstract

Two Schiff base ligands, 4-(((4-ethylphenyl)imino)methyl)phenol (4EMP) and (E)-4-((naphthalen-2-ylimino)methyl)phenol (4NMP) were synthesized by the reaction of 4-hydroxybenzaldehyde with 4-ethylaniline, 4EMP, or naphthalene-2-amine, 4NMP. The compounds were characterized using NMR (¹H and ¹³C), Fourier transform infra-red (FTIR) and mass spectroscopic techniques. The proton NMR identified the OH peaks at 9.73 and 9.77 ppm for 4EMP and 4NMP respectively, while the ¹³C-NMR showed the imine carbons at 172.57 ppm for 4EMP and at 160.89 ppm for 4NMP. The FTIR spectra showed characteristic peaks at 1605 cm⁻¹ (4EMP) and 1600 cm⁻¹ (4NMP) typical of the azomethine group, and the mass spectra results gave molecular ion peaks of 226.12 and 248.10 respectively. The structures of the compounds were further established by single crystal X-ray analysis. The corrosion inhibition potential of the compounds were studied on mild steel surface in a 1 M hydrochloric acid (HCl) solution, and was analysed using potentiodynamic polarization (PDP) and electrochemical impedance spectroscopy (EIS). The results of the

electrochemical methods showed that the studied molecules imparted high resistance in allowing flow of electrons across the metal–electrolyte platform and behaved as mixed type inhibitors with 4EMP showing better inhibition properties than 4NMP. Scanning electron microscopy (SEM) showed the formation of film on the mild steel surface. Quantum chemical calculations achieved by density functional theory (DFT) was further applied to explain the adsorption as well as inhibition abilities of the molecules on the mild steel surface. Thermodynamics studies showed that the two compounds obeyed the Langmuir isotherm with 4EMP conforming to chemisorption mechanism while 4NMP involved competitive physisorption and chemisorption mechanism.

Keywords: Schiff base; crystal structure; DFT; corrosion inhibition

1. Introduction

Schiff bases are important category of compounds which could serve as functional models for the elucidation of structures of biomolecules and biological processes [1]. They are often used as important ligands especially the ones bearing N, O, S donor atoms which exhibit structural similarities with neutral biological systems [2-4]. One of their structural significance has been the inherent interpretation of the mechanism of transformation of racemization reaction in biological systems attributed to the imine group (C=N). They also serve as one of the most relevant synthetic ligand systems, with importance in asymmetric catalysis, conducting materials and polymers, crystal engineering and therapeutic agents [5, 6]. Schiff bases have proven to be cheap starting precursors with relatively easy synthetic route. The high purity, low toxicity, and eco-friendliness have made the synthesis and structural studies of new Schiff base compounds very interesting.

In the last few years, extensive efforts have been made, both in academics and industry to develop Schiff base compounds with interesting anti-corrosion effect, because of their high thermal stability, complex forming ability and semiconducting properties [7]. Thus, it is the first step in the search for compounds with potentials to protect the surfaces of metal from environmental and chemical deterioration. Saha *et al.* [8] have evaluated the contributions of the species present in the molecules of (E)-4-((2-(2,4-dinitrophenyl)hydrazono)-methyl)pyridine, (E)-4-(2-(pyridin-4-ylmethylene)hydrazinyl)benzotrile and (E)-4-((2-(2,4-dinitro-phenyl)hydrazono)methyl)phenol towards the corrosion inhibition performances on

mild steel in 1 M HCl medium. Hamani *et al.* [9] investigated the corrosion inhibition effect of some new azomethine compounds on mild steel in 1 M HCl using potentiodynamic polarization, electrochemical impedance spectroscopy (EIS) and quantum chemical analysis. It was inferred that the inhibition efficiency increased with increasing inhibitor concentration and the Schiff bases function as mixed-type inhibitors with the adsorption patterns typical of Langmuir isotherm. Pordel *et al.* [10] reported that the intramolecular charge transfer (ICT) present in (5-hydrox-yimino-1-alkyl-4,5-dihydro-1H-4-indazolyliden)-2-arylacetonitriles due to the colour intensities could be potential sites for corrosion inhibition properties.

Mild steel is widely used in industries especially in petroleum sector for the transport of the crude and refined products, and they undergo corrosion with time due to attack by acid or basic solutions used in pickling. In order to reduce damage and achieve higher life time of the mild steel, corrosion inhibitors are needed for lower iron dissolution. The incessant environmental degradation associated with the use of inorganic corrosion inhibitors such as chromate and nitrite have shifted focus to the more environmental friendly organic counterparts [11-14]. Stringent environmental legislations and huge penalty for defaulters put in place by various national agencies, suggest the need to combat corrosion-related problems in industries holistically. Over the past two decades, extensive research and development have focused on the use of greener and smarter means to combat corrosion. Macrocyclic ligands containing N, S, O and P heteroatoms have also been found to possess broad spectrum anticorrosion properties [15-20]. The nature of the inhibiting molecules, steric effect, aromaticity, electron concentration on donor sites, type of orbitals donating electrons, presence of functional groups (such as N=N, C=N, C=S, C=C, R-OH, R=R), surface area of the molecule, molecular weight of the compound, temperature of reaction and potential effect at the metal/solution interface contribute immensely to the enhanced anti-corrosive properties of an inhibitor [22-26]. Recently, Nwankwo *et al.* [21], explored the corrosion inhibition properties of 1,8-dimethyl-1,3,6,8,10,13-hexaazacyclotetradecane ligand for mild steel in 1 M HCl.

In the quest to explore the behaviour of atoms and molecules, quantum chemical calculations have become a useful method to study reaction mechanism, determine the molecular structure, and equally elucidate the electronic structure and reactivity of compounds. More so, the study of corrosion inhibition mechanism in a compound has been made easy by this technique [27-29]. The possibility of quantum calculations are due to Density Functional

Theory (DFT) which is reliable and gives correct values for necessary parameters even for huge complex molecules at low cost, and could explain microcosmic inhibition performance and their reaction mechanism [30]. Thus, it has become a main source for connecting some traditional empirical concepts with quantum mechanics, and can be used to understand the interaction occurring at the material interface and analyse experimental data [31].

In the light of the interesting chemistry of Schiff base and their wide applications, we herein report the synthesis of two Schiff base compounds which were characterized using spectroscopic methods and single X-ray analysis. The corrosion inhibition potentials of the Schiff-base molecules in an aggressive acidic medium were studied using potentiodynamic polarization and electrochemical impedance spectroscopy (EIS) techniques. In addition, quantum chemical calculations were performed in order to gain required insights into their potential mechanism of inhibition. In this perspective, several quantum chemical properties such as E_{HOMO} , E_{LUMO} , energy gap (ΔE), electronegativity (χ), softness (σ), fraction of electron transferred from inhibitor to metal surface (DN) were studied.

2. Experimental procedures

2.1 Materials

The chemical reagents used for the synthesis and corrosion studies are of analytical grade. 4-ethylaniline, naphthalene-2-amine and 4-hydroxybenzaldehyde were purchased from Sigma-Aldrich and used without further purification. Ethanol, hydrochloric acid (32%) and acetone were purchased from Merck, South Africa.

2.2 Instrumentation

NMR spectra were recorded on a Bruker Avance III spectrophotometer operating at 600 MHz. DMSO- d_6 was used as solvent, and all chemical shifts (δ) are given in parts per million (ppm). Infrared spectra were measured on a Bruker alpha-P FTIR spectrophotometer in the frequency range 4000 – 400 cm^{-1} . Melting points were measured by using a Stuart Scientific melting Apparatus. The mass spectra of the ligands were recorded in ethanol solution in the positive ionization mode on a micrOTOF-Q 11 10390 Bruker compass Mass spectrometer. Electrochemical studies using potentiodynamic polarization and electrochemical impedance spectroscopic measurements were carried out using Autolab PGSTAT 302N obtained from Metrohm. The instrumental set up includes a three-electrode system; mild steel, platinum rod

and Ag/AgCl with 3 M KCl as working, counter and reference electrodes respectively. The surface analysis of the mild steel was carried out using Quanta FEG 250 Environmental scanning electron microscope (ESEM) under an acceleration voltage of 30 kV with simultaneous recording of the energy dispersive spectrum (EDS).

2.3 Synthesis of 4-(((4-ethylphenyl)imino)methyl)phenol and (E)-4-((naphthalen-2-ylimino)methyl) phenol Schiff bases

4-ethylaniline (10 mM) was added slowly to 1.22 g 4-hydroxybenzaldehyde (10 mM) dissolved in 40 mL ethanol, and drops of glacial acetic acid were added. In a similar procedure, 1.43 g of 1-naphthylamine (10 mmol) and 1.22 g of 4-hydroxybenzaldehyde (10 mmol) in 40 mL absolute ethanol was refluxed for 2 h, also in the presence of a few drops of glacial acetic acid. The solutions were filtered and slow evaporation resulted into shiny crystals suitable for single crystal X-ray analysis.

4EMP, Yield: 75.2%. m.p 156-160 °C. selected FTIR (cm^{-1}): 2962, 2929, 2871 ν ($\underline{\text{H}}\text{-C-C}$), 1605 ν (C=N), 1574, 1511 ν (C=C), 1411 σ (-C=C-N), 1309 ν (C-O), 1284, 1191(Ar-OH), 828(p-benzene ring). $^1\text{H-NMR}$: (DMSO, δ ppm): 1.13, 1.17 (m, CH_3), 2.38, 2.41(d, CH_2), 6.45, 6.87, 6.91, 7.11, 7.19, 7.61, 7.74 (m, C_6H_4), 8.43 (s, N=CH), 9.73 (s, OH). $^{13}\text{C-NMR}$ (DMSO, δ ppm): 15.51(CH_3), 28.81(CH_2), 114.15, 120.95, 126.56, 141.44, 146.55, 150.63, 159.33, 163.88(C_6H_4), 172.57(HC=N). MS (ESI) $m/z = \text{C}_{15}\text{H}_{15}\text{NO}$. Calcd 225.29. Found $[\text{M}+\text{H}]^+ = 226.12(100\%)$. Anal. cal for $\text{C}_{15}\text{H}_{15}\text{NO}$: C, 79.97% ; H, 6.71%; N, 6.22%; Found: C, 80.24%; H, 5.95%; N, 6.30%.

4MNP Yield: 65.4%. m.p 194-198 °C. selected FTIR (cm^{-1}): 3046 ν ($\underline{\text{H}}\text{-C=C}$), 2978, 2871 ν ($\underline{\text{H}}\text{-C-C}$), 1600 ν (C=N), 1580, 1567, 1515 ν (C=C), 1442 σ (-C=C-N), 1383 ν (C-O), 1284, 1152 (O-H), 1039 (aromatic C-H), 831, 772 (naphthalene rings). $^1\text{H NMR}$ (DMSO, δ ppm): 6.91, 6.93 (d, C_6H_4), 7.17, 7.54, 7.75, 7.91, 8.25 (m, C_{10}H_7), 8.52 (s, N=CH), 9.77 (s, OH). $^{13}\text{C NMR}$ (DMSO, δ ppm): 115.83, 123.59, 125.75, 125.10, 126.46, 133.61, 131.01, 148.93 (C_{10}H_7), 112.97, 127.77, 127.70, 128.55 (C_6H_4), 160.37 (HC=N), 160.89 (C-OH).

MS (ESI) $m/z = \text{C}_{17}\text{H}_{13}\text{NO}$ Calcd. 247.29. Found $[\text{M}+\text{H}]^+ = 248.10 (100\%)$. Anal. Calc. for $\text{C}_{17}\text{H}_{13}\text{NO}$: C, 82.57; H, 5.30; N, 5.66; Found: C, 81.19; H, 5.10; N, 6.33%.

2.4 Specimen preparation

Mild steel coupons with percentage weight composition: 0.17 % C, 0.46 % Si, 0.017 % S, 0.019 % P, and Fe of the remaining percentage was used for corrosion studies. Coupons of the mild steel material were made by cutting it into 1 cm x 1 cm and inserted in a Teflon holder using epoxy resin, with surface area of 1 cm² been exposed. Before the electrochemical measurement, there was proper cleaning of the mild steel surface by abrasion on Struers MD PianoTM 220 (size: 200) mounted on Struers LaboPol-1 machine. The surface was thoroughly cleaned to achieve a mirror-like surface. The mirror like coupons were cleaned in a sonicating acetone bath for 30 min, followed by sonication in ethanol, and subsequent cleaning with paper towel and dried. After drying, the mild steel was used for the corrosion studies. The aggressive medium of analysis (1 M HCl) was made from (32%) acid solution. The inhibitor concentrations: 40, 60, 100, 500 and 1000 ppm were prepared in mixture of acetone and ethanol, and remainder, distilled water and sonicated.

2.5 Mild steel surface analysis

The surface abraded mild steel strips of size 1 × 1 cm were immersed in 1 M HCl both in a medium without the inhibitor and with 100 ppm inhibitor for 3 h. Adequate cleaning of the surface with water, acetone and ethanol was done after the time of immersion. The sample was dried and analysed with SEM. Chemical composition of the mild steel (MS) surface was recorded by an EDS detector.

2.6 X-ray crystallography

Typical X-ray diffraction studies were carried out at 200 K using a Bruker Kappa Apex II diffractometer with graphite monochromated Mo K α radiation ($\lambda = 0.71073 \text{ \AA}$). The procedural data collection, cell refinement and data reduction were done by APEXII and SAINT programs [32]. SHELXT-2014 was used to solve the structures and refined by least-squares procedures with SHELXLE [33] as a graphical interface. The H-atoms attached to the carbons were placed in calculated positions and were included in the refinement in the riding model approximation, with $U_{\text{iso}}(\text{H})$ set to $1.2U_{\text{eq}}(\text{C})$ while the none-H atoms were anisotropically corrected. The methyl hydrogens were made to rotate with a fixed angle around the C—C bond to appropriately fit the experimental electron density (HFIX 137 in the

SHELX program suite [34]), with $U_{\text{iso}}(\text{H})$ set to $1.5U_{\text{eq}}(\text{C})$. In the case of the hydroxyl H-atom, rotation with a fixed angle around the C—O bond was done to best fit the experimental electron density (HFIX 147 in the SHELX program suite [34]), with $U_{\text{iso}}(\text{H})$ set to $1.5U_{\text{eq}}(\text{O})$. The obtained data were corrected for absorption effects by the numerical method using SADABS [32].

2.7 Quantum chemical calculations

Quantum chemical calculations were performed using density functional theory (DFT) method on a B3LYP (Becke's Three parameter hybrid functional using the LYP correlation functional) theoretical model with electron basis set 6-31G +(d, p) for all atoms [35]. Calculations were performed on the neutral molecules with Gaussian 09 [36]. The molecular geometries were taken directly from the X-ray diffraction experimental results without any constraints. Geometry optimization and various quantum chemical parameters were obtained. The quantum chemical parameters E_{HOMO} , E_{LUMO} , energy gap ΔE ($E_{\text{LUMO}} - E_{\text{HOMO}}$), chemical potential (μ), absolute electronegativity (χ), absolute hardness (η), global softness (σ), and the fraction of electrons transferred (ΔN) were obtained using the following equations [37-39]:

$$\text{Ip(ionization potential)} = -E_{\text{HOMO}} \text{ and } E_{\text{A}} \text{ (electron affinity)} = -E_{\text{LUMO}} \quad (1)$$

$$\text{Chemical potential, } \mu = -\frac{1}{2}(I_{\text{p}} + E_{\text{A}}) \quad (2)$$

$$\text{Absolute electronegativity, } \chi = -\frac{1}{2}(E_{\text{HOMO}} + E_{\text{LUMO}}) \quad (3)$$

$$\text{Absolute hardness, } \eta = -\frac{1}{2}(E_{\text{HOMO}} - E_{\text{LUMO}}) \quad (4)$$

$$\text{Energy gap, } \Delta E = E_{\text{LUMO}} - E_{\text{HOMO}} \quad (5)$$

$$\text{Global softness } (\sigma) = \frac{1}{\eta} \quad (6)$$

$$\text{Number of e- transferred from the inhibitor to metal surface } (\Delta N) = \frac{\chi_{\text{Fe}} - \chi_{\text{inh}}}{2(\eta_{\text{Fe}} + \eta_{\text{inh}})} \quad (7)$$

(In equation 7, $\chi_{\text{Fe}} = 7$ while $\eta_{\text{Fe}} = 0$).

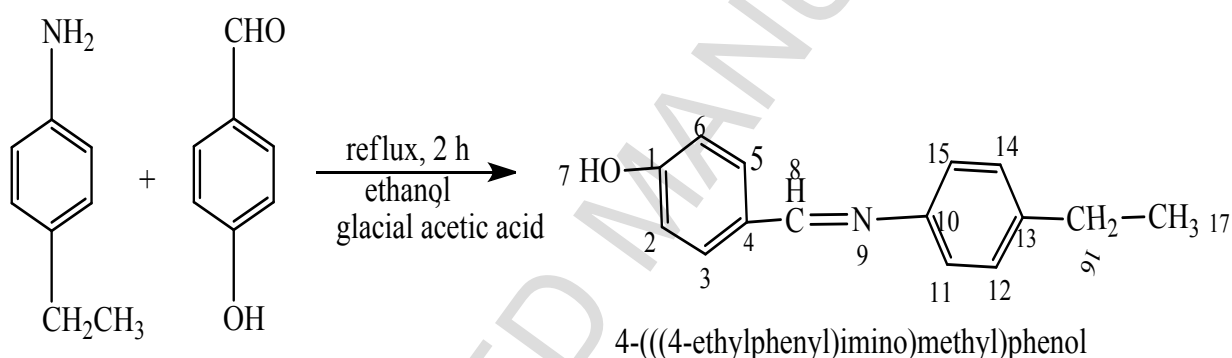
In a bid to ascertain the prospective centres of the inhibitor molecules that are prone to electrophilic attacks by the metallic atoms, the electron density surfaces of the electrophilic

Fukui function (f^-) of the studied Schiff bases were visualized using the Multiwfn software [40].

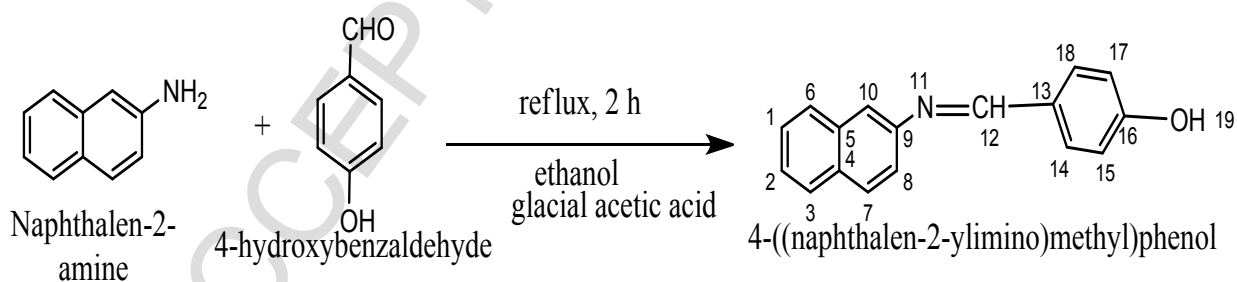
3. Results and Discussion

3.1 Synthesis

The results of the reaction of 4-ethylaniline with 4-hydroxybenzaldehyde in a 1:1 molar ratio in ethanol gave 4EMP as shown in scheme 1; while the reaction of naphthalene-2-amine with 4-hydroxybenzaldehyde readily gave 4MNP, both were obtained in moderately high yield (Scheme 2). The reaction was completed after 2 h and slow evaporation of the product solution afforded brownish yellow and brown crystals for 4EMP and 4MNP respectively. Both compounds were soluble in DMSO, hot ethanol and methanol, partially soluble in chloroform and ethyl acetate but insoluble in water and toluene.



Scheme 1: The synthetic pathway for 4-(((4-ethylphenyl)imino)methyl)phenol



Scheme 2: Reaction pathway showing the formation of (E)-4-((naphthalen-2-ylimino) methyl) phenol Schiff base

3.2 FTIR Spectral studies

The Infra-red spectroscopic studies of 4EMP show three peaks around 2962, 2929 and 2871 cm^{-1} which are characteristic of alkane homologues due to the CH_2CH_3 functional groups. These bands are weak and correspond to C-H stretching vibrations. The sharp peak observed at 1605 cm^{-1} could be attributed to $-\text{C}=\text{N}$ group and the peaks at 1574, 1511 and 1411 cm^{-1} are attributed to $-\text{C}=\text{C}-$ and C-H in plane bending vibrations of the aromatic ring which forms an important part of the molecule [41, 42, 43]. The band around 1309 cm^{-1} could be due to aryl OH deformations while 1284 and 1191 cm^{-1} , which were among the strongest peaks in the spectra, may be due to C-O stretching vibrations. The sharp and intense band at 828 cm^{-1} could be ascribed to out of plane vibrations of the p-disubstituted benzene ring [41, 44, 45].

In the spectra of 4MNP, bands due to the azomethine and the phenolic groups modes were observed. In addition, a few bands due to C-C stretching and symmetric/ asymmetric C-H modes also appeared. The bands at 3046 cm^{-1} may be assigned to the OH group, while the weak bands at 2978 and 2871 cm^{-1} could be due to the C-H stretching vibrations which are characteristics of the heteroaromatic structure. The absence of strong bands within 1600-1750 cm^{-1} range indicates the absence of carbonyl group, a consequence of the formation of the Schiff base. The appearance of strong bands in the region of 1515–1600 cm^{-1} could be assigned to the imine ($\text{C}=\text{N}$) group [46, 47]. Intense band that appeared at 1442 cm^{-1} could be due to the C-C stretching of the benzene and naphthalene rings and also the C-H in-plane bending modes of the aromatic rings [41, 45]. The bands which occurred around 1383-1152 cm^{-1} represent the C-O stretch, the O-H deformation which may have resulted from the phenolic group in the compound and CH_2 wagging and CH_2 twisting vibrations [41]. Within this region, also, aromatic C-H in-plane bending vibrations were observed with weak-to-medium intensities around 1039 cm^{-1} . The characteristic substituent patterns and also out of plane vibrations of the naphthalene rings could also be attributed to the band at 831 cm^{-1} [45].

3.3 ^1H NMR and ^{13}C NMR spectroscopy

The nuclear magnetic resonance analysis of the two compounds gave characteristic signals that conform to the structures. The ^1H NMR spectrum of 4EMP reveals the presence of protons of $\text{C}=\text{NH}$ group as one-proton singlet at 8.43 ppm. The observed singlet at 9.73 ppm could be due to the proton of the OH group attached to the aromatic molecule (Ar-OH), the appearance of this peak in the downfield region could be due to the inherent hydrogen

bonding present in the compound [48]. The resonant peaks due to the aromatic protons appeared as multiplets in the region 6.45 to 7.74 ppm [49, 50]. The ^{13}C NMR spectrum showed signals at 15.51 and 28.81 ppm corresponding to the sp^3 (CH_3) and sp^2 (CH_2) carbons of the ethyl substituent respectively. The signals due to the aromatic carbons were observed between 114.15- 163.88 ppm. Among the aromatic carbons, C-1 and C-10 resonated downfield (159.33 and 163.88 ppm respectively) compared to others due to their proximity to the electronegative atoms [51]. These two carbons also displayed shorter peaks which is characteristic of quaternary carbons. The carbon atoms: C2 and C6, C3 and C5, C8 and C12, C9 and C11 are equivalent carbons and presented the same resonant frequencies, thus same signals were observed. The resonance signal for the $\text{C}=\text{N}$ was observed at 172.57 ppm.

The ^1H -NMR spectrum of 4NMP showed a singlet at 8.52 ppm which can be ascribed to the imine proton $\text{HC}=\text{N}$. A singlet at 8.25 ppm may be due to the 10-H atom which might have experienced deshielding effect of the electronegative nitrogen atom located at β -position; and thereby resonated at higher δ -values than the other aromatic protons. The multiplets of peaks in the region of 7.54-7.91 ppm could be ascribed to some of the aromatic protons. The signal at 9.77 ppm could be attributed to the hydrogen atom of the OH group, whose high resonance frequency value could be due to hydrogen bonding thereby raising the signal to higher values [45].

The ^{13}C -NMR spectra of the compound exhibited bands almost at the same position (160.89 and 160.37 ppm) attributed to imine ($\text{HC}=\text{N}$) carbon and the C-16 attached to the OH. The band located at 148.93 ppm could be attributed to the carbon which is at α -position to the N-atom (C-9). The proximity to the imine group subjects it to the deshielding effect, hence resulting into higher resonance frequency (δ -values) compared to other C-atoms in the naphthalene ring. This peak appeared short compared to others because the carbon atom is a quaternary carbon. The signals observed in the up-field region in the range 112.97–133.61 ppm, are due to the aromatic carbons.

3.4 X-ray crystallography

Figure 1a presents the thermal ellipsoid representations of the compound 4EMP, while the schematic drawing of the crystal packing are presented in Figure 1b. The crystal structure of the compound is orthorhombic with space group $\text{Pca}21$. The molecule contains the iminophenolic ring and the ethylbenzene ring. In the asymmetric unit there are four molecules of

the compound. The structure is non-planar with the least square plane through the phenol ring making a dihedral angle of $52.03(10)^\circ$ with the least square plane through the ethylbenzene ring. In turn the ethyl group makes an angle of $73.8(3)^\circ$ with the ethylbenzene ring. The bond length of C(1)–N(1) ($1.282(3) \text{ \AA}$) is shorter than the length of normal C–N (1.47 \AA) and very close to that of C=N ($1.273(2) \text{ \AA}$) and C=N ($1.2437(5) \text{ \AA}$) [52].

There is one intermolecular O1—H1A...N1ⁱ (i: $1/2+x, 1-y, z$) interaction of length 1.89 \AA which links adjacent molecules and can be described with a $C^1_1(8)$ graph-set descriptor on the unary level [53, 54]. There is no short $\pi \dots \pi$ ring interactions, but there are two long C—H... π ring interactions with hydrogen to centroid length of 2.73 and 2.98 \AA with the rings of the phenol and ethylbenzene rings respectively. The bond lengths and angles are within normal ranges and they are comparable with those of related structures [55-57].

The ortep view and the crystal packing of 4MNP, drawn for the clearest view, are displayed in Figures 2a and b respectively. The compound crystallized in monoclinic system with space groups $P21/c$. In the asymmetric unit there are also four molecules of the compound. The structure of 4MNP is similar to another reported structure recorded at room temperature [58]. The structure is non-planar with the least square plane through the phenol ring making a dihedral angle of $54.96(4)^\circ$ with the least square plane through the naphthalene group. The bond distance obtained for N1 to C1 (C=N) is (1.2805 \AA) which is within the interval reported for other Schiff bases derived from naphthylamine such as the enol-imino (1.28 \AA) and keto-imino tautomer (1.30 \AA) [59]. Analysis of the torsion angles for the C20–N1–C1–C11 fragment and C20–C21–C22–C23 show values 178.89 and 179.30 (11) respectively which were the largest recorded values for the synthesized Schiff base. The slightly higher value for C20–C21–C22–C23 may be due to the OH group in the para position leading to a little steric effect. There is one long intramolecular C22—H22...N1 hydrogen interaction of 2.55 \AA . There is also an intermolecular O1—H1A...N1ⁱ (i: $-x, 1/2+y, 3/2-z$) interaction of length 1.93 \AA which links adjacent molecules and can be described with a $C^1_1(8)$ graph-set descriptor on the unary level [60, 61]. This intermolecular hydrogen bond contributes to the crystal packing, promotes proton transfer and at the same time, contributes to the rigidity of the molecule. The shortest $\pi \dots \pi$ ring interaction is between naphthalene groups with an inter-centroid distance of $3.7755(7) \text{ \AA}$ and a slippage of 0.789 \AA . The phenol group has on each side a C—H... π ring interaction with hydrogen to centroid distances of 2.70 and 2.77 \AA . The crystal packing is governed by hydrogen bond and C–H... π interactions.

Details of crystal data and structure refinements for the two compounds are provided in Table

1, while selected bond lengths and bond angles are shown in Tables 2 and 3 respectively.

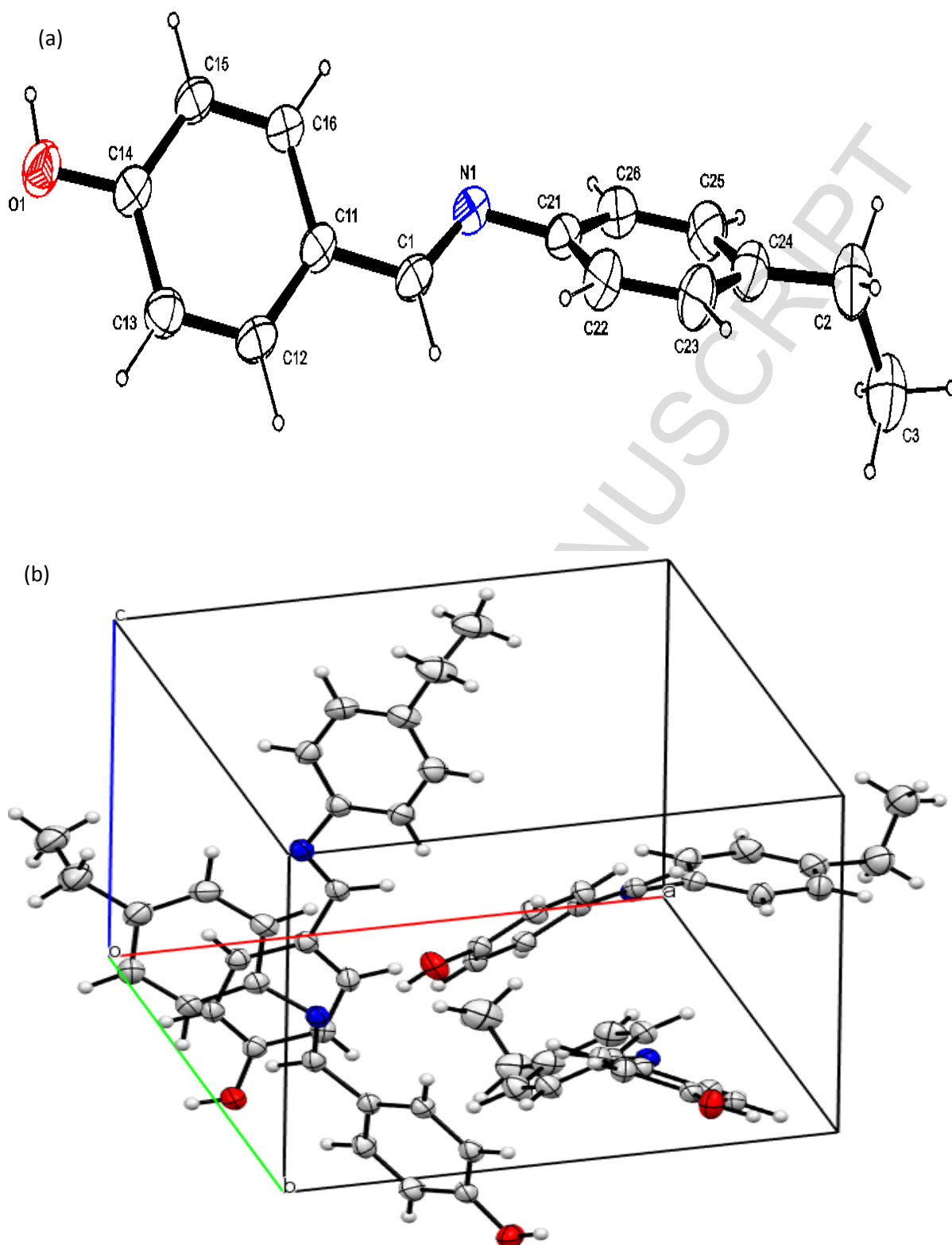


Figure 1: (a) The molecular structure, and (b) crystal packing of 4-(((4-ethylphenyl)imino)methyl)phenol with displacement ellipsoids drawn at 50% probability level

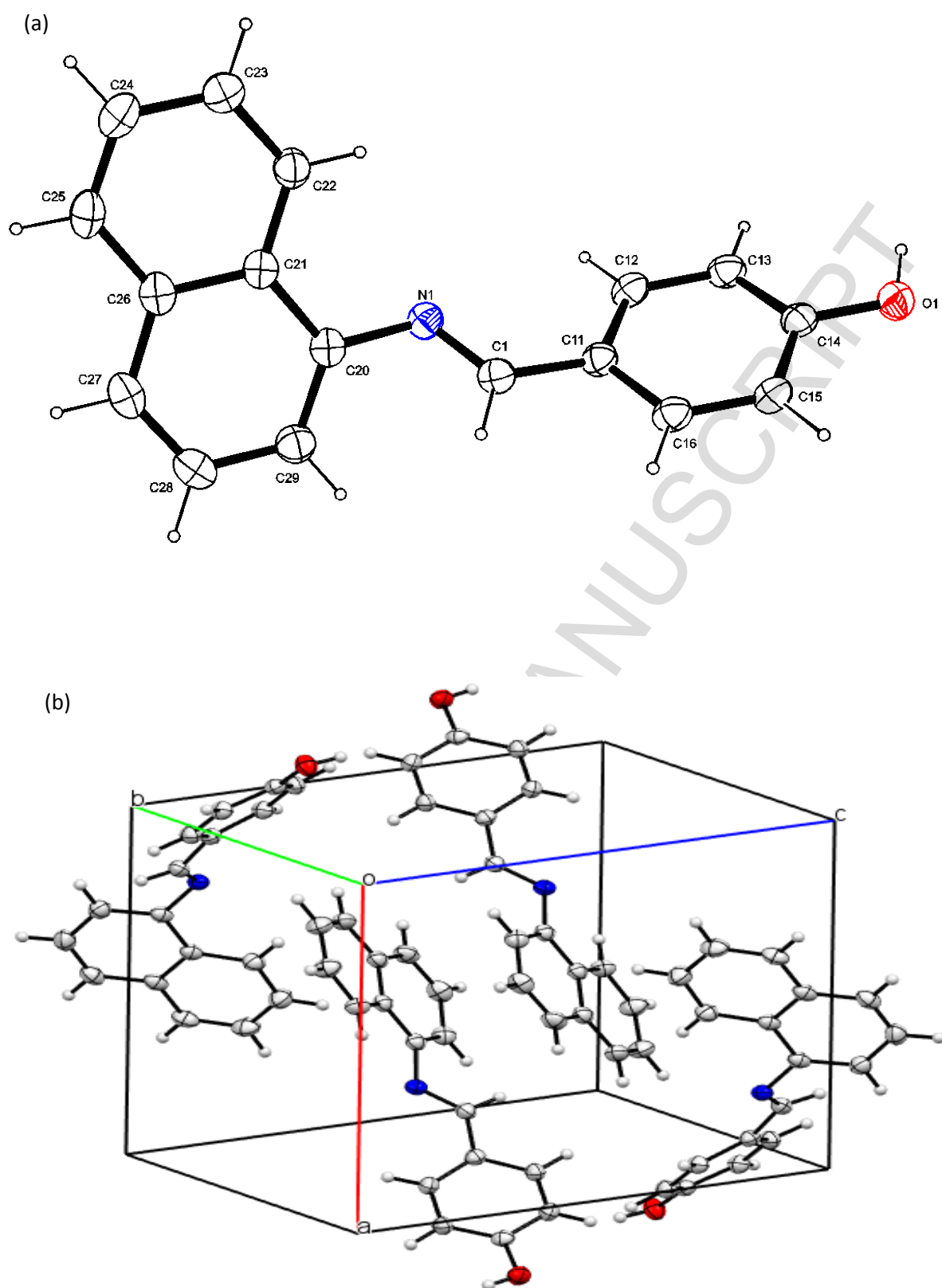


Figure 2: (a) The molecular structure, and (b) crystal packing of (E)-4-(naphthalene-2-ylimino)methylphenol with displacement ellipsoids drawn at 50% probability level

Table 1: Crystal structure data of 4EMP and 4MNP

Compound	4EMP	4MNP
CCDC	1491359	1490099
Empirical formula	C ₁₅ H ₁₅ NO	C ₁₇ H ₁₃ NO
Colour/shape	Yellowish-brown/needle-like	Brown
Formular weight	225.28 g/mol	247.28 g/mol
Temperature (K)	200	200
Crystal system	orthorhombic	monoclinic
Space group	Pca21	P 21/c
a/Å	10.9790(6)	9.9811(5)
b/Å	11.7326(6)	10.4585(6)
c/Å	9.2365(5)	11.9435(7)
V/Å ³	1189.77(11)	1245.34(12)
Z	4	4
Density _{cal} /g/cm ³	1.258	1.319
Absorption coefficient (μ)/mm ⁻¹	0.079	0.082
F(000)	480	520
Crystal size/mm ³	0.23 x 0.41 x 0.58	0.26 x 0.42 x 0.51
Radiation (Å)	0.71073	0.71073
Θ _{min} , Θ _{max} (°)	3.4, 28.3	3.2, 28.3
Dataset	-12:14, -15:15, -12:12	-13:12, -13:13, -15:15
Total uniq data, R(int)	24923,2907,0.018	21781,3069,0.016
R ₁ ^a (I > 2σ(I))	2747	2675
R, wR ₂ , S	0.0367, 0.0986, 1.07	0.0373, 0.1038, 1.06
Min and Max resd.dens.(e/ Å ⁻³)	-0.20,0.24	-0.21,0.25

Table 2: Selected bond lengths and angles for 4EMP

Bond lengths		Bond angles	
O(1)-C(14)	1.344(2)	C(1)-N(1)-C(21)	118.84(16)
N(1)-C(1)	1.282(3)	C(14)-O(1)-H(1A)	109.00
N(1)-C(21)	1.424(2)	N(1)-C(1)-C(11)	123.88(17)
O(1)-H(1A)	0.8400	C(3)-C(2)-C(24)	113.8(2)
C(1)-C(11)	1.462(3)	C(1)-C(11)-C(12)	119.07(17)
C(2)-C(3)	1.507(4)	C(1)-C(11)-C(16)	122.62(18)
C(2)-C(24)	1.519(4)	N(1)-C(21)-C(22)	122.44(17)

Table 3: Selected bond lengths and angles for 4NMP

Bond lengths		Bond angles	
O(1)-C(14)	1.3506(13)	C(1)-N(1)-C(20)	117.65(9)
N(1)-C(1)	1.2805(13)	C(14)-O(1)-H(1A)	109.00
N(1)-C(20)	1.4264(13)	N(1)-C(1)-C(11)	125.56(9)
O(1)-H(1A)	0.8400	O(1)-C(14)-C(15)	117.67(9)
C(24)-C(25)	1.3651(17)	C(1)-C(11)-C(12)	124.76(9)
C(12)-H(12)	0.9500	C(23)-C(22)-H(22)	120.00
C(22)-H(23)	0.9500	C(21)-C(26)-C(25)	118.45(10)

3.5 Quantum chemical methods

In the light of classical chemical considerations, interactions involving a compound and other species are either by electrostatic or orbital system. The **distribution** of electrons and their movement bring about electrostatic interactions within molecules and are true reflections of their chemical reactions and physico-chemical properties [62, 63]. Figure 3 shows the optimized geometry, the HOMO density distribution, and the LUMO density distribution of 4EMP and 4NMP molecules as obtained using DFT at the B3LYP/6-31G+ level of theory.

The interest in DFT quantum chemical technique has grown due to the understanding of atoms and molecular dynamics, their structural behaviour, properties and reactivities including clusters and different agents [64]. Further information on Figures 3 shows an even distribution of electrons on the HOMO and LUMO part of the molecules, which could be due to the presence of nitrogen and oxygen atoms and several π -electrons on the entire molecules creating the platform for adsorption by active centres. It is critical to divulge that the ethyl alkyl chain of 4EMP is not involved in the LUMO distribution. The molecules present interesting active sites that have strong ability to form coordinate bond with the empty d-orbital of the iron. The N and O atoms have lone pairs of electrons which bond with the unfilled 3d orbitals of the iron metal thereby creating protective molecular surface film. The back donation from the metal atom to the LUMO of the inhibitor molecules creates an interfacial barrier that would resist the further attack of the metal surface by corrosion agents [65].

The obtained quantum chemical parameters (such as E_{HOMO} , E_{LUMO}) and electron density distribution over the frontier molecular orbitals (FMOs) reflect an effective action of the synthesized compounds as good inhibitors compared to previous reports [39, 65]. Ju *et al.* [65] reported the corrosion inhibition of some oxadiazoles and from their quantum chemical calculations, the obtained energy gap was higher than the obtained value in this work with lower dipole moments. Similarly, the reports of Yadav *et al.* [39] on corrosion inhibition of benzimidazoles derivatives also showed large energy gaps from their quantum calculations ranging from 7.947 to 8.059 eV with higher dipole moments (3.20-5.02) and lower fraction of electrons transferred (0.27-0.29). Our results are comparable to the report of Saha *et al.* [66], in which the fraction of electrons transferred using their Schiff base molecules as inhibitors ranged from 0.7377-0.7529 and the energy gaps recorded were 3.3846-3.9517 eV.

Other parameters calculated in this work as shown in Table 4 such as absolute hardness and softness are important properties that measure stability and reactivity of the molecules. Hard molecules are characterised by large energy gap while soft molecule possess small energy gap [67]. In terms of reactivity, soft molecules are more reactive than hard ones since they have small energy gap that can enable the easy transfer of electrons. **This trend is however consistent with ones observed in the literature and only provides for a qualitative agreement.** It has been reported that effective corrosion inhibitors are molecules that can both donate electrons to unoccupied orbital of the metal and equally accept free electrons from the metal

[68]. The two molecules could be categorized as good corrosion inhibitors from theoretical studies perspective.

From the calculated absolute softness (σ), 4NMP can be taken as a soft molecule compared to 4EMP and it has lower energy gap thereby placing it as a more reactive compound than 4EMP. On the contrary, experimental corrosion results from impedance spectra shows that at 100 ppm, the % inhibition efficiency of 4EMP is 93% while that of 4MNP is 55%. This shows that there are some limitations to theoretical. Further explanation to such contrasting behaviour could be that, the adsorption on the metal surface based on the quantum calculations, electrochemical and crystallographic studies occurred in different modes according to the molecular structures. One of such is chemisorption which involves sharing of lone pair electrons between electronegative atoms and the mild steel. Other modes are through intermolecular force reflecting physisorption, which is relevant to the dipole of the inhibitor and the plane conjugating system of the aromatic ring, which donate π -electrons to the metal surface, accept electrons from the metal surface and intercalation of hyperconjugating system [69].

Fukui function f^- was employed to analyse the relative susceptibility of the active atomic sites of an inhibitor molecule to electrophilic attacks. According to Nwankwo *et al.* [70], the favourable site for electrophilic attack is the atom in the molecule where the value of f^- is the highest. From the isosurface density of the Fukui function (f^-) shown in Figure 3, the electron density distributions of the f^- revealed that the O-atoms of the OH groups and the C=C π -electrons centres of the benzene rings in both 4NMP and 4EMP are the most susceptible sites for electrophilic attacks in the molecules. In addition, the N-atoms and the ethyl alkyl chain attached to the C=C π -electrons centres are also susceptible to electrophilic attacks.

Optimized structures

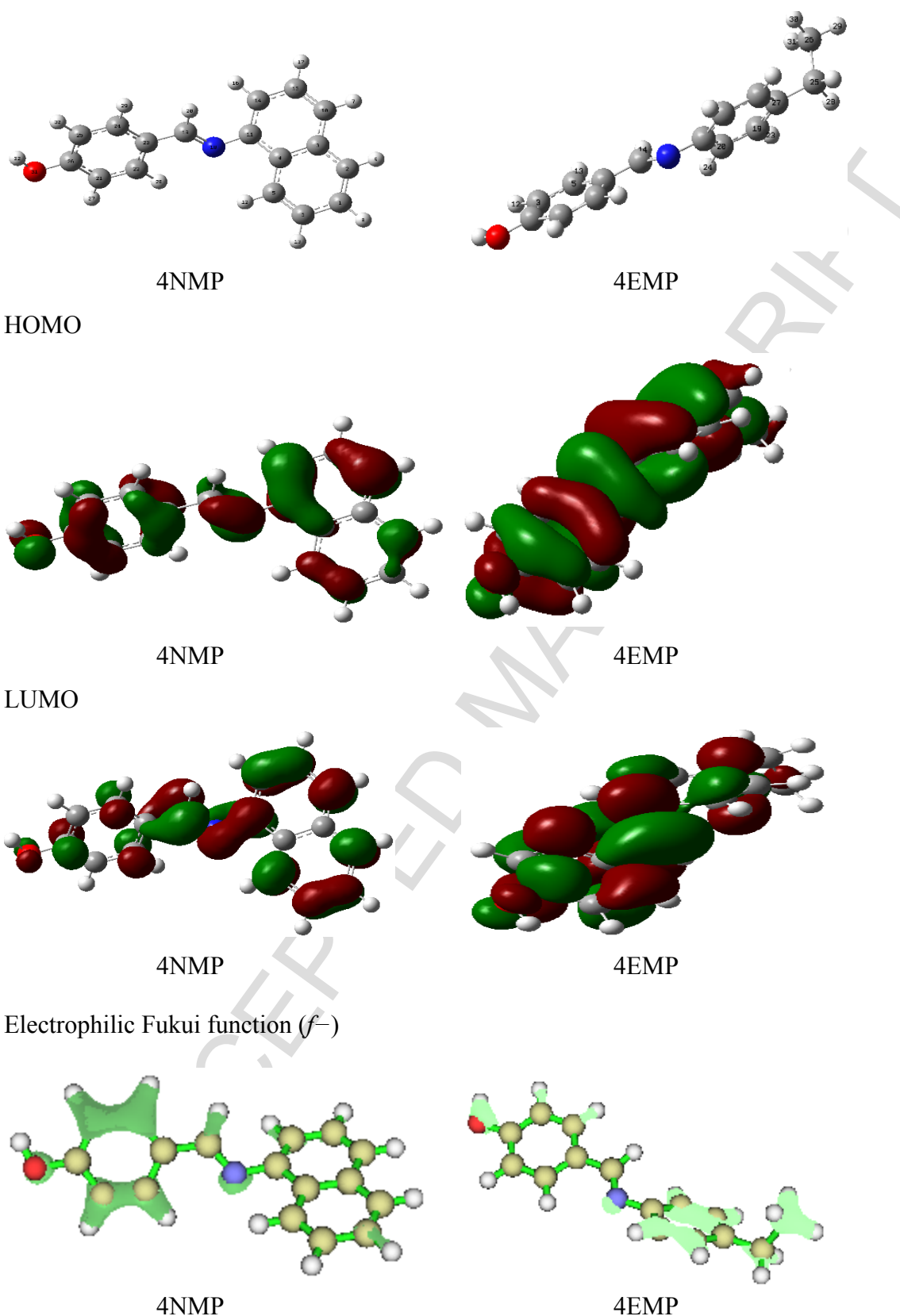


Figure 3: Optimized molecular structures for 4NMP and 4EMP with atom numbering, HOMO, LUMO electron density isosurfaces and the electrophilic Fukui function (f^- , isosurface value = 0.15) of compounds obtained at B3LYP/6-31G+(d,p) level of theory.

Table 4: Calculated quantum chemical parameters

Parameters	4NMP values(eV)	4EMP values(eV)
E_{HOMO}	-5.630	-5.901
E_{LUMO}	-1.862	-1.722
ΔE	3.767	4.178
Ionization potential(I_p)	5.630	5.900
Electron affinity(E_A)	1.862	1.722
Chemical potential (μ)	-3.746	-3.811
Absolute electronegativity(η)	3.746	3.811
Absolute softness(σ)	0.531	0.479
Absolute hardness (χ)	1.884	2.089
Fraction of electron transferred(ΔN)	0.864	0.763

3.6 Thermodynamic considerations and adsorption isotherms

Adsorption isotherms provide reliable information about the nature of interactions that exist at the metal/solution interface where both the water and inhibitor molecules are present [71]. It is a well-known fact that the most probable mechanism by which organic compounds inhibit metal dissolution is by adsorbing onto the metal surface [21]. In a bid to unravel the adsorptive characteristics of the studied Schiff bases, the data generated from EIS were tested using Freundlich and Langmuir isotherms.

The general equations for the adsorption models are:

$$\text{Freundlich isotherm: } \theta = K_{ads} C_{inh} \quad (13)$$

$$\text{Langmuir isotherm: } \frac{C_{inh}}{\theta} = \frac{1}{K_{ads}} + C_{inh} \quad (14)$$

where, θ is the degree of surface coverage; K_{ads} is the equilibrium constant of the adsorption/desorption process and C_{inh} is the concentration of the inhibitor. However, both isotherms do not conform to the expected conditions where the Freundlich adsorption model in Equation 13 expects intercept at $\theta = 0$ and the slope of the Langmuir adsorption isotherm in Equation 14 should be unity. The deviation of the slope of a Langmuir adsorption plot from unity has been attributed to possible interactions between the adsorbed inhibitor

molecules [72]. As a result, a modified form of the Langmuir isotherm which is not possible with the Freundlich isotherm was employed to calculate K_{ads} and ΔG_{ads} values. The plots of the models are shown in Figures 4a-d for both 4EMP and 4NMP. The modified form of Langmuir isotherm is given in equation 15:

$$C_{inh}/\theta = 1/K_{ads} + mC_{inh} \quad (15)$$

In this modified model, m is the slope of the plot and can be assumed to be an inherent factor in the surface coverage values. The intercept of the plots was then equated to $(1/m)K_{ads}$, from which K_{ads} was calculated. The K_{ads} and ΔG_{ads} values are 1611.43 and 28.72 kJ/mol for 4NMP, and 767.28×10^6 and 61.7 kJ/mol for 4EMP respectively. The reasonably high value of K_{ads} obtained for 4EMP in the present study suggests strong adsorption of its molecule on the metal surface [72].

The change in Gibb's free energy of adsorption (ΔG_{ads}) was calculated by using the equation:

$$\Delta G_{ads} = -RT \ln(55.5K_{ads}) \quad (16)$$

where ΔG_{ads} is the standard free energy of adsorption; R is the gas constant and T is the absolute temperature. The value of 55.5 is the concentration of water in solution in molL^{-1} . The ΔG_{ads} values obtained for 4NMP lies between threshold of -20 kJmol^{-1} (for physisorption) and -40 kJmol^{-1} (for chemisorption) which corroborates that the studied Schiff base molecule adsorb on mild steel surface in 1 M HCl via competitive physical and chemical adsorption mechanisms [70] while for 4EMP, the value of ΔG_{ads}^0 obtained was reasonably above -40 kJmol^{-1} . This showed electronic transfer from the compound to the mild steel thereby creating coordinate covalent interaction. Such value of ΔG_{ads}^0 for the adsorption of 4EMP ligand on MS surface in 1 M HCl therefore, suggests strong chemisorption mechanism [21, 73]. In addition, the negative sign alludes to the spontaneity of the adsorption process [70].

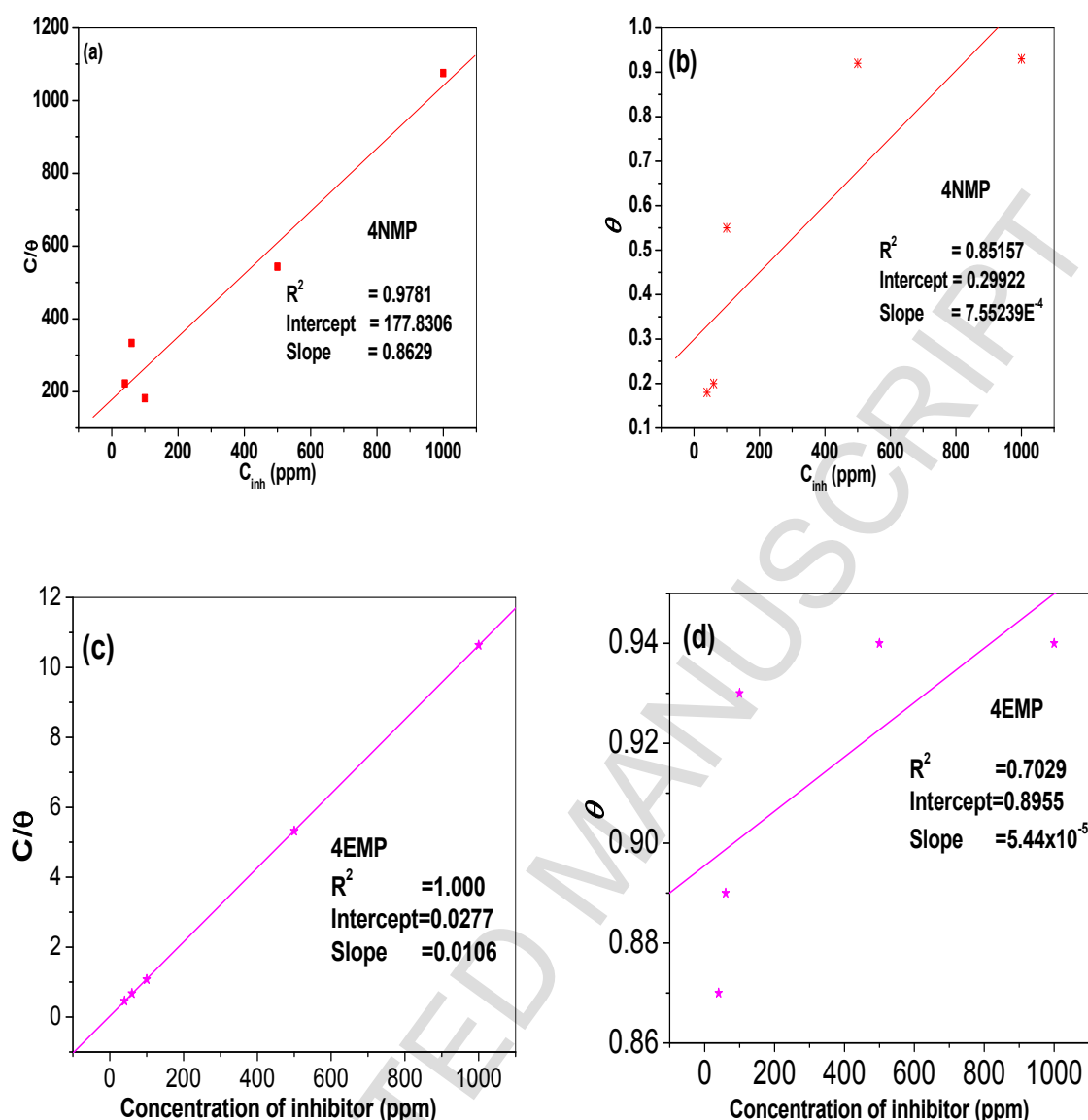


Figure 4: Representative adsorption isotherms for MS in 1 M HCl containing various concentrations of the Schiff base: (a,c) Langmuir (b,d) Freundlich.

3.7. Electrochemical measurements

3.7.1. Potentiodynamic polarization (PDP) study.

The effect of the inhibitor concentration on the anodic and cathodic polarization behaviour of mild steel in 1 M HCl solution has been investigated using polarization measurements and the recorded Tafel plots are shown in Figure 5. The respective kinetic parameters derived from the above plots are given in Table 5. The data from the Tables shows that both anodic metal dissolution of iron and cathodic hydrogen evolution reaction were significantly inhibited after the addition of the inhibitor compounds to 1 M HCl solution, and such behaviour is attributed

to an excellent mixed-type inhibitor. Meanwhile, the effects on both anodic and cathodic reactions were significantly enhanced at elevated concentrations of the two Schiff bases. The inhibition of these reactions became more pronounced on increasing the concentration between the thresholds of 40 to 1000 ppm. The values of corrosion current density (i_{corr}) recorded for 4EMP show that at a very low concentration (40 ppm), inhibitor recorded a significant drop, which suggests that the studied inhibitor performed greatly in protecting mild steel surface in 1 M HCl better than 4NMP which recorded similar corrosion current density at almost 500 ppm. The insignificant shift in E_{corr} values as opposed to i_{corr} indicates that the investigated compounds prevent the corrosion process by forming a protective film without necessarily altering the reaction mechanism [74].

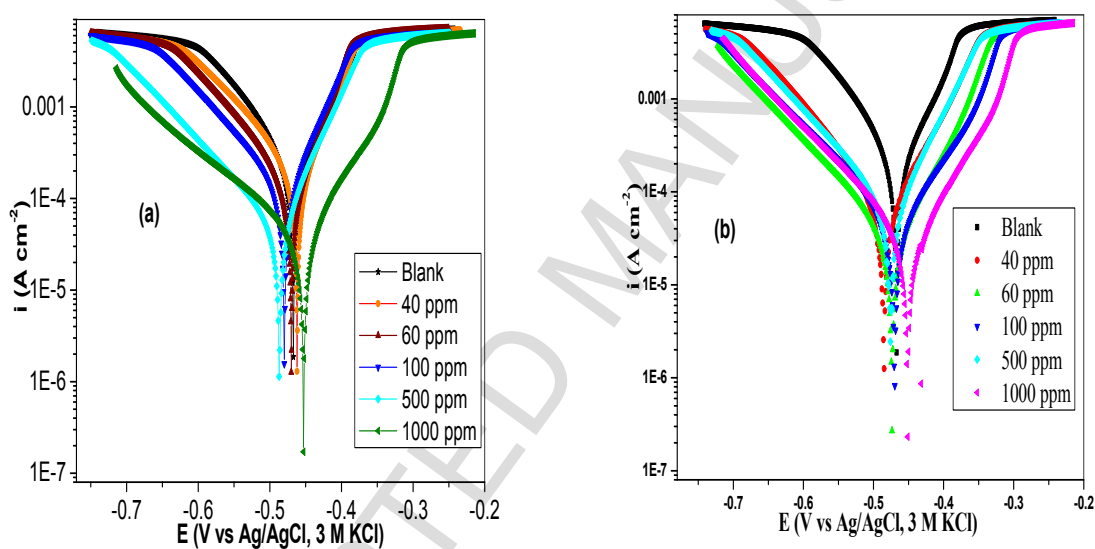


Figure 5: Polarization curves for MS in absence and presence of different concentrations of inhibitors: (a) 4NMP and (b) 4EMP.

Table 5: Tafel polarization parameters for MS in 1 M HCl solution in absence and presence of different concentrations of the studied 4NMP and 4EMP

Conc (ppm)	b_a (mV/dec)	b_c (mV/dec)	$-E_{\text{corr}}$ (mV)	i_{corr} ($\mu\text{A cm}^{-2}$)	$\eta\%$	θ
Blank	98.93	72.08	452.72	236.22	-	-
4NMP						
40	111.47	61.93	461.92	193.56	18.1	0.18
60	118.32	61.52	469.96	182.27	22.8	0.23
100	85.10	58.64	479.68	100.82	57.3	0.57
500	47.57	71.11	486.70	24.70	90	0.90
1000	127.48	67.14	452.94	20.20	91	0.91
4EMP						
40	69.48	65.38	485.12	34.59	85	0.85
60	109.87	76.28	473.65	29.30	88	0.88
100	68.85	103.89	473.65	25.05	89	0.89
500	74.47	62.12	475.55	24.75	90	0.90
1000	78.63	73.99	451.35	17.43	93	0.93

3.7.2. Electrochemical impedance spectroscopic (EIS) studies.

The characteristics and kinetics of electrochemical reactions which takes place at metal-solution interface can interestingly be verified using the electrochemical impedance spectroscopy [74]. Nyquist plots for the mild steel immersed in 1 M HCl solution in the absence and presence of the compounds are shown in Figure 6, while impedance parameters, such as, solution resistance (R_s), charge transfer resistance (R_{ct}), constant phase element (Y_0), the phase shift (n) and the calculated inhibition efficiency (η) values are listed in Tables 6. The Table shows that R_{ct} values increased and significantly so at high concentrations of the inhibitor compounds. In addition, at 1000 ppm inhibitor concentration for 4EMP and 4NMP, larger diameter semicircles were obtained than the other four lower concentrations (Figure 6). The impedance spectrum recorded at each condition could be seen to give diminished capacitive imperfect semicircles in high frequency region, which reflects charge transfer and

protective film formation on the mild steel [21]. The imperfect semicircles are due to mass transfer processes, frequency dispersion and contributing effect of roughness of metal surface [21]. In this report, the impedance characteristics of mild steel corrosion was probed in a simple electrical equivalent circuit matrix with a resistor of solution resistance (R_s), a resistor of charge transfer (R_{ct}) and a constant phase element (CPE). CPE has successfully been employed for the description of depressed semicircles with their origin below the real axis [75]. The impedance nature of CPE is defined as follows [74]:

$$Z_{CPE} = \left(\frac{1}{Y_0} \right) [(j\omega)^n]^{-1} \quad (17)$$

where, Y_0 is the CPE constant; ω is the angular frequency ($\omega = 2\pi f_{\max}$) at which the imaginary part of the impedance ($-Z''$) is maximal; j is the imaginary number and n is the phase shift (exponent). The phase shift serves as a determinant of the heterogeneity or roughness of the mild steel surface [75]. In general, CPE can be expressed by the values of n , for instance, if resistive ($n = 0$, $Y_0 = R$), capacitive ($n = 1$, $Y_0 = C$), inductive ($n = -1$, $Y_0 = L$) and Warburg impedance ($n = 0.5$, $Y_0 = W$) [73]. From this study, n ranges from 0.76 to 0.83 for 4EMP and 0.80-0.84 for 4NMP.

Figure 7 shows the Bode plots for mild steel in 1 M HCl without and with different concentrations of the inhibitors. A close observation of the Bode plot of 4NMP system reaffirms poor inhibitory action of the inhibitor at lower concentrations due to diminished adsorptive strength of the molecule on steel surface. This was evident on the absence of phase angle maxima observed for the 4NMP system at lower concentrations. The figures however show that at higher frequency, the values of $\log |Z|$ and phase angle approaches zero. Such phenomenon is a characteristic response of resistive behaviour that can be attributed to solution resistance enclosed between the reference electrode (Ag/AgCl, 3 M KCl) and working electrode (mild steel) [76, 77]. At intermediate frequencies for 4EMP, however, a linear relationship between $\log |Z|$ vs. $\log f$ with a slope near -1 and the phase angle approaching -70 can be observed. This could be seen as a shift from the ideal capacitive behaviour at intermediate frequencies since slope of -1 and a phase angle of -90 defines ideal capacitive behaviour [74, 75]. For 4NMP, reasonable pseudo-capacitive behavior could only be achieved at maximum inhibitor concentration as revealed in Table 6. That is, at lower concentrations, 4NMP recorded slope values lower than the blank system.

The slopes of the Bode plots at intermediate frequencies (S) and the maximum phase angles (α) for MS in 1 M HCl solution at minimum and maximum concentrations of 4EMP and 4NMP are listed in Table 6. The deviation from an ideal capacitive behaviour is often attributed to rough working electrode [74]. In addition, the Bode plots shown in Figure 7 are characterized by single maximum (one time constant) at intermediate frequencies which is slightly broadened in the presence of inhibitors, thus suggesting the formation of a protective film on the mild steel surface [74].

The change observed in the values of R_{ct} and Y_0 can be related to the gradual removal of water molecules by the inhibitor compound on the electrode surface, which consequently resulted to decrease in the number of active sites available for the corrosion process [75].

Figure 8 presents the equivalent circuit employed for the fitting of impedance data for the studied corrosion inhibitors.

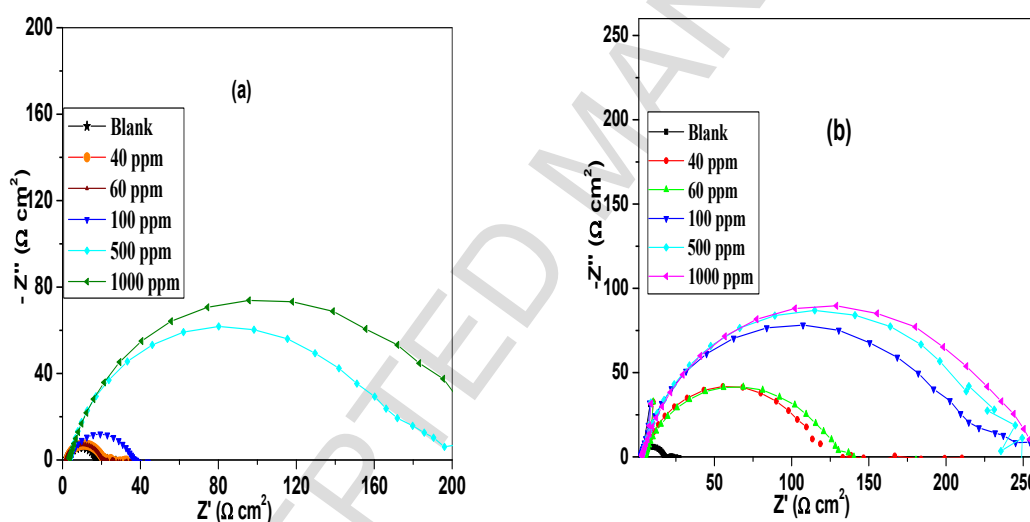


Figure 6: Nyquist plots (a) 4NMP and (b) 4EMP for MS in 1 M HCl in the absence and presence of different concentrations of inhibitors.

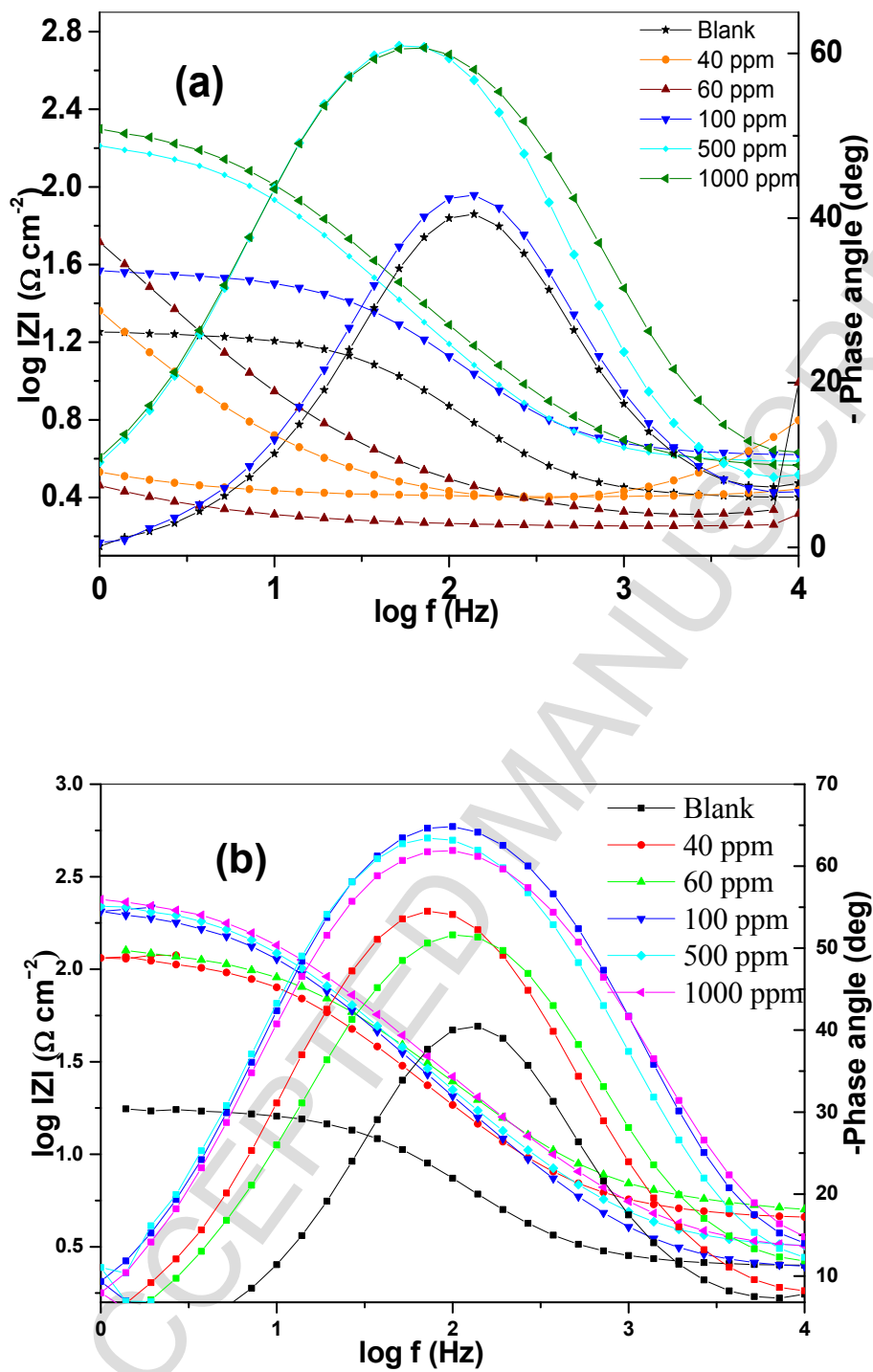


Figure 7: Bode plots for MS in 1 M HCl in absence and presence of different concentrations of (a) 4NMP and (b) 4EMP.

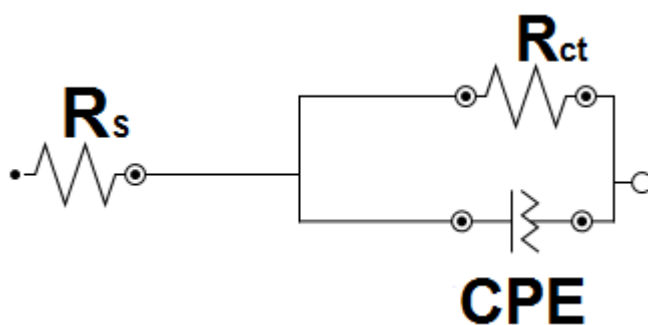


Figure 8: Equivalent circuit used to fit the EIS spectra.

Table 6: Electrochemical impedance parameters obtained for MS in 1 M HCl in absence and presence of different concentrations of 4NMP and 4EMP.

Inhibitor Conc (ppm)	R_s	R_{ct}	Y_0	n	η %	$-S$	$-\alpha$
Blank	2.50	16.6	677	0.84	-	0.53	40.47
4NMP							
40	2.52	20.3	890	0.84	18.2	0.29	42.94
60	1.80	20.8	793	0.84	20.2		
100	4.07	37.2	457	0.81	55.4		
500	3.73	197	316	0.83	92.0		
1000	3.45	250	303	0.80	93.0	0.98	60.68
4EMP							
40	4.49	129	296	0.82	87.0	0.64	54.51
60	4.68	149	308	0.76	89.0		
100	2.33	249	231	0.83	93.0		
500	3.08	261	213	0.83	94.0		
1000	2.95	293	215	0.80	94.0	0.80	61.91

3.8 Mild steel surface analysis

The surface examination by SEM and related EDX spectra for MS in the absence and presence of the Schiff bases are shown in Figures 9a-c. Figures 9(a) shows MS surface in 1 M HCl and Figures 9(b) and (c) show MS surface in 1 M HCl containing 100 ppm of 4EMP and 4NMP inhibitors. The MS immersed in 1 M HCl solution showed a highly damaged, rough and eroded surface full of corrosion products. The observed bumps like features, pits and cavities were due to acid attack. However, the specimen immersed in the inhibitor solutions showed improved surface with passive film as well as conditioning layers and little roughness

due to physical abrasion during metal preparation and cleaning. The observed passive films on the mild steel surfaces in the presence of inhibitor were composed of carbonaceous materials emanating from treatment with inhibitor molecules.

For 4EMP, the EDX data reveals the following elemental percentages: C(10.44%), O(2.37%), Al(0.15%), S(0.1%), Fe(86.94%) for the inhibited sample; C(6.86%), O(23.99%), Cl(34.6%), Fe(34.55%) for the uninhibited sample while for 4MNP, the EDX data for the treated surface is as follows: C(7.4%), O(2.34%), Al(0.08%), S(0.21%), Fe(89.96%). The high content of Fe in the treated surface as compared to the untreated surface revealed the extent of inhibition and protection offered by the Schiff bases. However, after immersed in 1.0 M HCl solution for 3 h, a very high chlorine content of 34.6% was observed due to the aggressive attack of acid solution but such was not observed with the inhibitor showing no formation of corrosion product ($\text{FeCl}_2 \cdot n\text{H}_2\text{O}$) on the MS surface [78, 79]. These values confirm the formation of protective layer by inhibitors on the MS surface in 1M HCl solution.

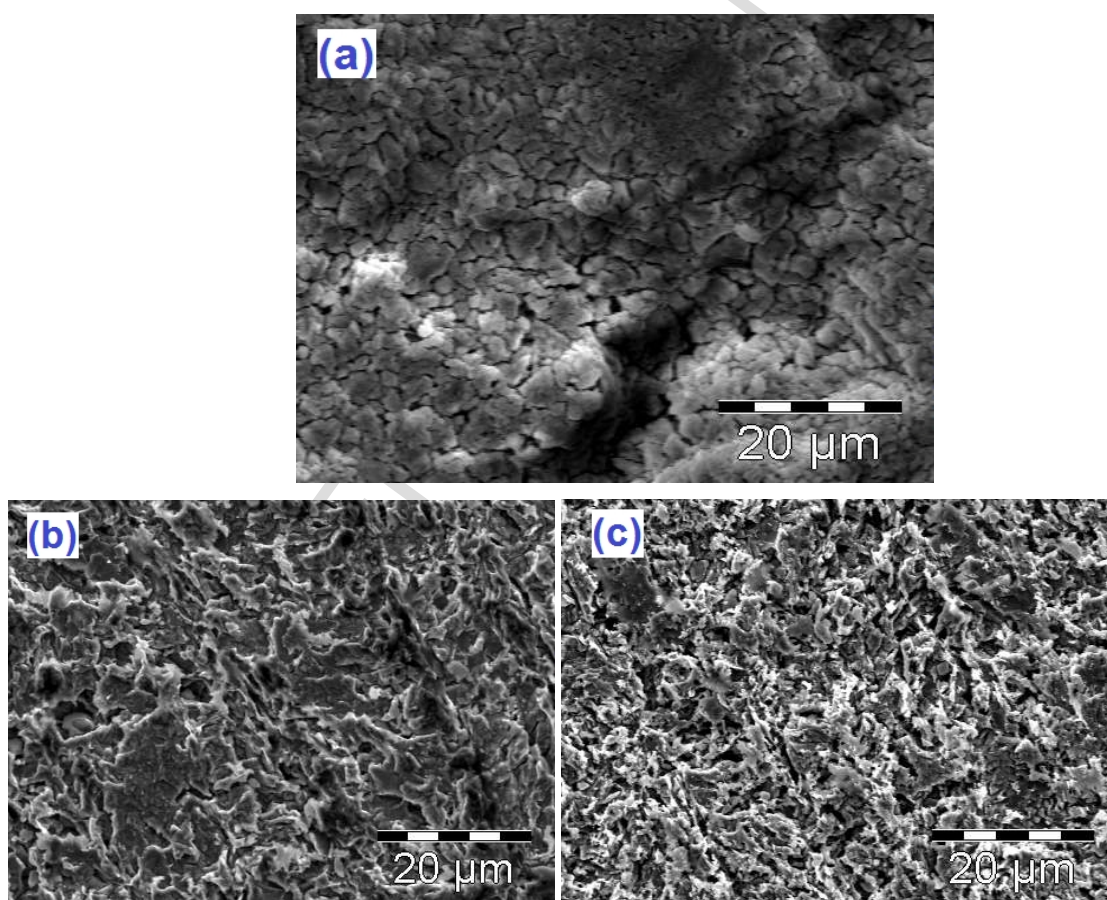


Figure 9: SEM images of MS surfaces (a) in 1 M HCl, (b) in the presence of 1 M HCl and 100 ppm of the 4EMP while (c) is for 4NMP.

4.0 Conclusion

Two Schiff base compounds 4EMP and 4NMP were synthesized and characterized by various spectroscopic techniques. The molecular structures of the compounds were further elucidated by X-ray diffraction analysis and theoretical calculations carried out by B3LYP/6-31 G+ (d,p) level of theory. The experimental results show that the 4EMP tends to be a better corrosion inhibitor than the 4NMP. From the theoretical modelling, the value of the energy separation between the HOMO and LUMO is not too large and could be compared to similar Schiff base compounds reported earlier. Moreover, we expected 4EMP to have lower energy gap than 4NMP according to the experimental results but the theoretical values was on the contrary signifying that the action of corrosion inhibitors involves complex steps.

To the best of our knowledge, these Schiff base compounds and their potential application in electrochemistry is reported for the first time in this work. The investigation of corrosion efficiency of the Schiff bases in acidic media could be summarised as follows:

1. Polarization curves proved that the inhibitor compounds are excellent mixed-type inhibitor at high concentrations for MS corrosion in 1 M HCl.
2. Electrochemical impedance spectroscopy plots indicated that the inhibitor increased the charge transfer resistance significantly, which supports that its inhibitory performance depended on the adsorption of the studied compounds on mild steel surface.
3. The adsorption of the inhibitor molecules was found to obey the Langmuir's isotherm with profound chemisorption mechanism for 4EMP and both physisorption and chemisorption for 4NMP.
4. The excellent performance of the studied inhibitors especially 4EMP for mild steel corrosion in 1 M HCl may be attributed to multiple factors including the presence of nitrogen and oxygen donor atoms, several π bonds and alkyl chain on its moiety that facilitated its easy adsorption.

In view of the results of our research, our approach will be helpful for quick prediction of a potential inhibitor from a lot of other reported inhibitors and subsequently offer rational design modification for enhanced corrosion inhibition application following a simplified chemical synthetic route.

Acknowledgment

EEE acknowledges North West University Mafikeng campus, South Africa for offering him a postdoctoral position and for providing the necessary facilities for this study. The authors acknowledge the efforts of the technicians, Department of Chemistry, North West University for all the assistance during the course of this work.

Supplementary materials

Crystallographic data for the structures reported in this paper have been deposited in the Cambridge Crystallographic Data Centre (CCDC) with reference numbers 1491359 and 1490099. Copies of the data can be obtained free of charge on application to the CCDC, Cambridge, UK (<http://www.ccdc.cam.ac.uk/>).

References

1. S.N. Pandeya, D. Sriram, G. Nath, E.D. Clercq, *Il Farmaco* 54 (1999) 628.
2. Y. Shibuya, K. Nabari, M. Kondo, S. Yasue, K. Maedo, F. Uchida, H. Kawaguchi, *Chem. Lett.* 37 (2008) 79.
3. A. Roth, J. Becher, C. Herrmann, H. Gorls, G. Vaughn, M. Reiher, D. Klemm, W. Plass, *Inorg. Chem.* 45 (2006) 10076.
4. E.Keskioglu, A.B.Gunduzalp, S.Cete, F.Hamurcu, B.Erk, *Spectrochim. Acta* 70A (2008) 640.
5. K.P. Bryliakov, E.P. Talsi, *J. Mol. Catal. A.* 264 (2007) 287.
6. J.D. Talati, M.N. Desai, N.K. Shah, *Mater. Chem. Phys.* 93 (2005) 64.
7. S. Hasnain, N. Nishat, *Spectrochim. Acta* 95A (2012) 457.
8. S. K. Saha, A. Dutta, P. Ghosh, D. Sukul, P. Banerjee, *Phys. Chem. Chem. Phys.* 18 (2016) 17911
9. H. Hamani, T. Douadi, M. Al-Noaimi, S. Issaadi, D. Daoud, S. Chafaa, *Corros. Sci.* 88 (2014) 245.
10. D. Arish, M.S. Nair, *Arabian J. Chem.* 5 (2012) 186.
11. I. Radojčić, K. Berković, S. Kovač, J. Vorkapić-Furać, *Corros. Sci.* 50 (2008) 1504.
12. P.C. Okafor, M.E. Ikpi, I.E. Uwah, E.E. Ebenso, U.J. Ekpe, S.A. Umoren, *Corros. Sci.* 50 (2008) 2317.
13. L.R. Chauhan, G. Gunasekaran, *Corros. Sci.* 49 (2007) 1161.
14. J. Halambek, K. Berković, J. Vorkapić-Furać, *Mater. Chem. Phys.* 137 (2013) 795.

15. M.A Quraishi, K.R. Ansari, E.E. Ebenso, *Int. J. Electrochem. Sci.* 7 (2012) 13120.
16. K. Babić-Samardžija, K.F. Khaled, N.Hackerman, *Appl. Surf. Sci.* 240 (2005) 340.
17. M.A. Quraishi, J. Rawat, *Mater. Chem. Phys.* 70 (2001) 99.
18. A. Singh, Y. Lin,; I.B. Obot, E.E. Ebenso, K.R. Ansari, M.A. Quraishi, *Appl. Surf. Sci.* 356 (2015) 347.
19. A. Singh, Y. Lin, M.A. Quraishi, L.O. Olasunkanmi, O. E. Fayemi, Y. Sasikumar, B. Ramagathan, I. Bahadur, I.B. Obot,; A.S. Adekunle,; M.M. Kabanda, E.E. Ebenso, *Molecules* 20 (2015) 15146.
20. M. Dibetsoe, L.O. Olasunkanmi, O.E. Fayemi, S.Yesudass, B. Ramagathan, I. Bahadur, A.S. Adekunle, M.M. Kabanda, E.E. Ebenso, *Molecules* 20 (2015) 15734.
21. H.U. Nwankwo, C.N. Ateba, L.O. Olasunkanmi, S. Abolanle, A.S. Adekunle, D.A. Isabirye, D.C. Onwudiwe, E.E. Ebenso, *Materials* 9 (2016) 20.
22. E.E. Oguzie, B.N. Okolue, C.E. Ogukwe, C. Unaegbu, *Mater. Lett.* 60 (2006) 3378.
23. L. Herrag, B. Hammouti, S. Elkadiri, A. Aouniti, C. Jama, H. Vezin, F. Bentiss, *Corros. Sci.* 52 (2010) 3051.
24. K.R. Ansari, M.A. Quraishi, A. Singh, *Corros. Sci.* 79 (2014) 15.
25. I.B. Obot, N.O. Obi-Egbedi, S.A. Umoren, *Corros. Sci.* 51 (2009) 282.
26. D.K. Yadav, M.A. Quraisha, B. Maiti, *Corros. Sci.* 55 (2012) 266.
27. G. Bereket, C. Ogretir, , C. Ozsahin, *J. Mol. Struct.* 663 (2003) 46.
28. K. F. Khaled, K. Babic-Samardzija, N. Harkerman, *Electrochim. Acta*, 50 (2005) 2520.
29. I. B. Obot, N. O. Obi-Egbedi, *Colloids Surf. 330A* (2008) 212.
30. M. S. Masoud, M. K. Awad, M. A. Shaker, M. M. T. El-Tahawy, *Corros. Sci.* 52 (2010) 2396.
31. E. E. Ebenso, T. Arslan, F. Kandemirli, N. Caner, I. Love, *Int. J. Quantum Chem.* 110, (2010) 1018.
32. APEX2, SADABS and SAINT, Bruker AXS Inc., Madison, Wisconsin, USA, 2010.
33. G. M. Sheldrick. A short history of SHELX. *Acta Cryst. A*64 (2008) 122.
34. C. B. Hübschle, G. M. Sheldrick, B. Dittrich. ShelXle: a Qt graphical user interface for SHELXL. *J. Appl. Cryst.* 44 (2011) 1284.
35. **W. Kohn, A.D. Becke, R.G. Parr, *J. Phys. Chem.* 100 (1996) 12980**
36. **M.J. Frisch, G.W. Trucks, H.B. Schlegel, G.E. Scuseria, M.A. Robb, J.R. Cheeseman, J.A. Montgomery, T. Vreven, K.N. Kudin, J.C. Burant, J.M. Millam, S.S. Iyengar, J. Tomasi, V. Barone, B. Mennucci, M. Cossi, G. Scalmani, N. Rega, G.A. Petersson, H.**

- Nakatsuji, M. Hada, M. Ehara, K. Toyota, R. Fukuda, J. Hasegawa, M. Ishida, T. Nakajima, Y. Honda, O. Kitao, H. Nakai, M. Klene, X. Li, J.E. Knox, H.P. Hratchian, J.B. Cross, V. Bakken, C. Adamo, J. Jaramillo, R. Gomperts, R.E. Stratmann, O. Yazyev, A.J. Austin, R. Cammi, C. Pomelli, J.W. Ochterski, P.Y. Ayala, K. Morokuma, G.A. Voth, P. Salvador, J.J. Dannenberg, V.G. Zakrzewski, S. Dapprich, A.D. Daniels, M.C. Strain, O. Farkas, D.K. Malick, A.D. Rabuck, K. Raghavachari, J.B. Foresman, J.V. Ortiz, Q. Cui, A.G. Baboul, S. Clifford, J. Cioslowski, B.B. Stefanov, G. Liu, A. Liashenko, P. Piskorz, I. Komaromi, R.L. Martin, D.J. Fox, T. Keith, M.A. Al-Laham, C.Y. Peng, A. Nanayakkara, M. Challacombe, P.M.W. Gill, B. Johnson, W. Chen, M.W. Wong, C. Gonzalez, J.A. Pople, Gaussian 03W, Revision E. 01, Wallingford, CT, Gaussian Inc (2004)
37. V. S. Sastri, J. R. Perumareddi, *Corrosion* 53 (1997) 622.
38. I. Lukovits, E. Klamann, F. Zucchi, *Corrosion* 57 (2001) 8.
39. M. Yadav, D. Behera, S. Kumar, R. R. Sinha, *Ind. Eng. Chem. Res.* 52 (2013) 6328.
40. T. Lu, F. Chen, *Multiwfn: a multifunctional wavefunction analyzer. J. Comput. Chem.* 33 (2012) 592.
41. Y.B. Shankar Rao, V. Veeraiah, T. Sundiusc, K. Chaitanya, *J. Mol. Str.* 10.1016/j.molstruc.2017.05.053
42. A. Goszczynska, H. Kwiecienc, K. Fijałkowski, *Med. Chem. Res.* 24 (2015) 3577.
43. S. Bal, B. Orhan, J. D. Connolly, M. Dgrak, S. Koytepe, *J. Therm. Anal. Calorim.* 121 (2015) 917.
44. P. V. Rao, A. V. Narasaiah, *Indian J. Chem.* 42A (2003) 1899.
45. W. Kemp, *Organic spectroscopy*, Macmillian press London, 71 (1991)
46. S. Destri, I.A. Khotina, W. Porzio, *Macromolecules*, 31 (1998) 1086.
47. S. Mini, V. Sadasivan, S.S. Meena, P. Bhatt, *Spectrochim. Acta.* 151A (2015) 604.
48. M. Hranjec, K. Starcevi, S. K. Paveli, P. Lucin, K. Paveli, G. K. Zamola, *Eur. J. Med. Chem.* 46 (2011) 2279.
49. R. M. Issa, S. A. Azim, A. M. Khedr, D. F. Draz, *J. Coord. Chem.* 62 (2009) 1870.
50. P.S. Reddy, *J. Chem. Pharm. Res.* 8 (2016) 79.
51. A. M. Nassar, A. M. Hassan, M. A. Shoeib, A. N. El kmash, *J. Bio. Tribo. Corros.* 1 (2015) 19.
52. A. Soltani, F. Ghari, A. D. Khalaji, E. T. Lemeski, K. Fejfarova, M. Dusek, M. Shikhi, *Spectrochim. Acta* 139A (2015) 278.

53. J. Bernstein, R. E. Davis, L. Shimoni, N.L. Chang, *Angew. Chem. Int. Ed. Engl.* 34 (1995) 1573.
54. M. C. Etter, J. C. MacDonald, J. Bernstein, *Acta Crystallogr.* B46 (1990) 262.
55. M. S. Alam, D. Lee *Spectrochim. Acta* 145A (2015) 574.
56. T. Doleck, J. Attard, F. R. Fronczek, A. Moskun, R. Isovitsch, *Inorg. Chim. Acta* 362 (2009) 3876.
57. O. Maury, J. P. Guégan, T. Renouard, A. Hilton, P. Dupau, N. Sandon, L. Toupet, H. L. Bozee, *New J. Chem.* 25 (2001) 1566.
58. L Ren-Yu Li, B. Feng-Li, Y. X. Xu-Jie Xing-You, L. Lu-De, W. Xin *Chin. J. Appl. Chem.* 20 (2003) 918.
59. A. Blagus, D. Cinčić, T. Friščić, B. Kaitner, V. Stilinović, *Maced. J. Chem. Chem. Eng.* 29 (2010) 138.
60. J. Bernstein, R. E. Davis, L. Shimoni, N. L. Chang, *Angew. Chem. Int. Ed. Engl.* 34 (1995) 1573.
61. M. C. Etter, J. C. MacDonald, J. Bernstein, *Acta Crystallogr.* 46B (1990) 256.
62. G. Gece, S. Bilgic, *Corros. Sci.* 52 (2010) 3443.
63. N.O. Obi-Egbedi, I.B. Obot. *Corros Sci.* 53 (2011) 275.
64. H. L. Madkour, S. K. Elrob, *Int. J. Ind. Chem.* 6 (2015) 184.
65. H. Ju, L. Ding, C. Sun, J. Chen, *Adv. Mat. Sci. Eng.* 2015 (2015) 5.
66. S. K. Saha, A. Dutta, P. Ghosh, D. Sukul, P. Banerjee, *Phys. Chem. Chem. Phys.* 17 (2015) 5690.
67. E.E. Elemike, H.U. Nwankwo, D.C. Onwudiwe, E.C. Hosten, *J. Mol. Struct.* 1141 (2017) 22.
68. E.E. Elemike, D.C. Onwudiwe, H.U. Nwankwo, E.C. Hosten, *J. Mol. Struct.* 1136, (2017) 262.
69. K.F. Khaled, *Electrochim. Acta* 53 (2008) 3484.
70. H.U. Nwankwo, L.O. Olasunkanmi, E.E. Ebenso, *Sci. Rep.* 7 (2017) 18.
71. S. Kumar, H. Vashisht, L. O. Olasunkanmi, I. Bahadur, H. Verma, G. Sigh, I.B. Obot,; E. E. Ebenso, *Scientific Reports* 6 (2016) 18.
72. N.O. Eddy, H. Momoh-Yahaya, E.E. Oguzie, *J. Adv. Res.* 6 (2015) 217.
73. A. Ostovari, S.M. Hoseinieh, M. Peikari, S.R. Shadizadeh, S.J. Hashemi, *Corros. Sci.* 51 (2009) 1949.
74. C. Verma, M.A. Quraishi, L.O. Olasunkanmi, E.E. Ebenso, *RSC Adv.* 5 (2015) 85430.
75. D.K. Yadav, M.A. Quraishi, B. Maiti, *Corros. Sci.* 55 (2012) 266.

76. M. Kissi, M. Bouklah, B. Hammouti, M. Benkaddour, *Appl. Surf. Sci.* 252 (2006) 4197
77. E. Naderi, A.H. Jafari, M. Ehteshamzadeha, M.G. Hosseini, *Mater. Chem. Phys.* 115 (2009) 858.
78. P. Zhao, Q. Liang, Y. Li, *Appl. Surf. Sci.* 252 (2005) 1607.
79. S. Saravanamoorthy, S. Velmathi, *Prog. Org. Coatings*, 76 (2013) 1535.

RESEARCH HIGHLIGHTS

- 4-(((4-ethylphenyl)imino)methyl)phenol and (E)-4-((naphthalen-2-ylimino) methyl) phenol were synthesized
- Crystal structures and spectral properties of the compound were reported.
- The reactivity of the molecule was elucidated from the quantum chemical calculations.
- The corrosion inhibition potential of the compounds were studied on mild steel
- Langmuir isotherm involved competitive physisorption and chemisorption mechanism